ELSEVIER

Computers and Chemical Engineering 24 (2000) 2417–2433

Computers & Chemical Engineering

www.elsevier.com/locate/compchemeng

Noninvertibility in neural networks

Ramiro Rico-Martínez [a], Raymond A. Adomaitis [b], Ioannis G. Kevrekidis [c,*]

[a] *Departamento de Ingeniería Química, Instituto Tecnológico de Celaya, Celaya, Gto. 38010 Mexico*
[b] *Department of Chemical Engineering, University of Maryland, College Park, MD 20742, USA*
[c] *Department of Chemical Engineering, School of Engineering & Applied Science, Princeton University, Olden Street, Princeton, NJ 08544-5263, USA*

Received 21 July 1999; received in revised form 30 May 2000; accepted 30 May 2000

Abstract

We present and discuss an inherent shortcoming of neural networks used as discrete-time models in system identification, time series processing, and prediction. Trajectories of nonlinear ordinary differential equations (ODEs) can, under reasonable assumptions, be integrated *uniquely* backward in time. Discrete-time neural network mappings derived from time series, on the other hand, can give rise to *multiple* trajectories when followed backward in time: they are in principle *noninvertible*. This fundamental difference can lead to model predictions that are not only slightly quantitatively different, but qualitatively inconsistent with continuous time series. We discuss how noninvertibility arises, present key analytical concepts and some of its phenomenology. Using two illustrative examples (one experimental and one computational), we demonstrate when noninvertibility becomes an important factor in the validity of artificial neural network (ANN) predictions, and show some of the overall complexity of the predicted pathological dynamical behavior. These concepts can be used to probe the validity of ANN time series models, as well as provide guidelines for the acquisition of additional training data.

Keywords: Noninvertibility; Artificial neural networks; Time-series processing; System identification

1. Introduction

Input/output mappings constructed using artificial neural networks (ANNs) are used extensively for nonlinear system identification. Both the short- and the long-term dynamic behavior of experimental systems can often be successfully predicted using such neural network-based approximations (see e.g. Weigend & Gershenfeld, 1993). By including one (or more) operating parameter(s) as input(s) to the network, the dependence of the dynamics on the parameter(s) can be studied. In particular, instabilities and transitions of the predicted long-term attractors (both local and global bifurcations) can be analyzed by varying the parameter in the resulting model and exploiting numerical bifurcation algorithms (see e.g. Kevrekidis, Rico-Martínez, Ecke, Lapedes & Farber, 1994).

When we study the predictions of a neural network as a function of the input parameter(s), we expect that not only the short term predictions, but also the long term attractors (their nature and bifurcations) should reflect those of the original system. If the physical system is described by a set of ordinary differential equations in time

$$\dot{\vec{X}} = \vec{f}(\vec{X};\vec{\gamma}), \qquad \vec{X}\in\mathcal{R}^q, \quad \vec{\gamma}\in\mathcal{R}^p, \quad \vec{f}:\mathcal{R}^q\times\mathcal{R}^p\mapsto\mathcal{R}^q \tag{1}$$

and the states of the system ($\vec{X}$) are recorded at discrete time intervals, $(n-1)\Delta t$, $n\Delta t$, $(n+1)\Delta t$,... a numerical integrator can be used to effectively construct a map between $\vec{X}_n$ and $\vec{X}_{n+1}$: i.e. given the complete state of the system $\vec{X}_n$ and the operating parameter values $\vec{\gamma}$, a call to an accurate numerical integrator will provide (after a number of integration steps to satisfy error control) an accurate estimate of $\vec{X}_{n+1}$. In completely analogous fashion, the equations can be integrated numerically backwards in time (the numerical integrator routine called with a negative time horizon) to provide a unique accurate estimate of $\vec{X}_{n-1}$. A numerical integrator can therefore be used to construct a map

* Corresponding author. Tel.: +1-609-2582818; fax: +1-609-2580211.
E-mail address: yannis@arnold.princeton.edu (I.G. Kevrekidis).

0098-1354/00/$ - see front matter
PII: S0098-1354(00)00599-8

$$\vec{X}_{n+1} = \vec{F}(\vec{X}_n;\vec{\gamma}) \tag{2}$$

as well as another map,

$$\vec{X}_{n-1} = \vec{G}(\vec{X}_n;\vec{\gamma}). \tag{3}$$

How close $\vec{F}\circ\vec{G}$ is to the identity is, of course, a measure of the accuracy and the *consistency* of the numerical integrator. In the context of this paper, the important point is that, given $\vec{X}_{n+1}$, backward in time integration provides a *unique* $\vec{X}_n$.

Consider now an ANN — with nonlinear activation functions — used to fit the 'one-step-ahead' map $\vec{F}$; such a network is trained using time series data (the complete state $\vec{X}_n$ of the system at some moment in time $(t_0 + n\Delta t)$, and the parameter values $\vec{\gamma}$ as inputs and the state $\vec{X}_{n+1}$ at time $(t_0 + (n+1)\Delta t)$ as target outputs). Inverting this network (in loose analogy with backward integration) should then provide (an estimate of) the pre-image $\vec{X}_{n-1}$ of $\vec{X}_n$. It should be clear that 'inverting the network' involves the solution of a set of coupled nonlinear algebraic equations (for nonlinear activation functions): given the network parameters (weights and thresholds), operating parameter value inputs ($\vec{\gamma}$), and the *output* $\vec{X}_n$, find the network inputs $\vec{X}_{n-1}$ consistent with the outputs. Since the actual trajectory is unique backward in time, one would also expect the trained network to be *uniquely invertible*. In other words, given the complete state $\vec{X}_n$ of the system at some moment in time $(t_0 + n\Delta t)$ we should be able to find a unique preimage of that point, since this is equivalent to integration of the differential equations backwards for the appropriate time interval. Since, however, nonlinear equations can have multiple solutions, discrete-time ANNs have a built-in noninvertible character!

Furthermore, inverting a discrete time neural network with sigmoidal (tan*h*-type) activation functions (using the output to find what values of the input are consistent with it) requires solving a set of (transcendental) nonlinear equations. In general, such equations will have an unknown number of solutions and one will not be able to obtain explicit expressions to compute them. In principle, any neural network allowing multiple preimages is *inconsistent* (globally in phase space) with a continuous-time dynamical system (a set of ordinary differential equation (ODEs)). In many cases, however, only one of the multiple preimages 'makes sense', and the other ones are far away in phase space (Rico-Martínez, Kevrekidis & Adomaitis, 1993; Rico-Martínez, Anderson & Kevrekidis, 1994a; Gicquel et al., 1998) (e.g. some preimages of a physical variable may have a negative value and are therefore not acceptable). In these cases, when only one 'relevant' preimage can be somehow singled out, one can still consider the network predictions to be valid *in a restricted region of phase space*. However, when *multiple* preimages fall within the relevant range of phase space, the dynamics of the iterated network take on features exclusively found in noninvertible maps, producing transitions and types of behavior qualitatively impossible for invertible dynamical systems (and therefore incorrect). It is important to note that the presence of noninvertible features does not necessarily imply that complex behavior *will* be observed. Nor is noninvertibility a necessary condition for complex behavior: for state space dimensions greater than two (for maps) and three (for ODEs) complex (chaotic) behavior may be the result of purely invertible mechanisms.

In previous work (Rico-Martínez et al., 1993), we studied an analogy between noninvertibility in one-step simple explicit integrator schemes and discrete-time neural networks. There, we suggested the use of noninvertible dynamics concepts as a tool for computing bounds on the valid range of the network predictions. Such an approach is different from standard cross-validation methods based on statistics of short-term predictions, which are not appropriate for detecting noninvertibility.

This paper presents illustrations of the pathologies that neural networks may exhibit due to their noninvertible character. These illustrations are based on two examples involving model development aimed at capturing a transition from steady-state to simple periodic behavior. The first case study centers on a neural network trained on experimental data; the second uses simulated data to show that noninvertibility may arise from factors other than experimental noise. Our brief description is not exhaustive, nor is it intended as a self-contained survey of noninvertible dynamical phenomena. The examples only attempt to serve as an illustration of the complexity of the phenomenology that a neural network may exhibit, associated with its noninvertible character. They should serve as a guide to the neural network practitioner in understanding the nature of some of the predictive behavior of neural network models. For readers familiar with nonlinear dynamics, we have included in our description certain technical details that highlight the bifurcation structure underlying the pathologies. We have tried to expose things in a way such that readers without this background can skip over these technical details and still sample the phenomenology in an informative manner. Those more interested in the nonlinear dynamics technical details should consult the references given through the text. Finally, we will attempt to offer some insights on ways to detect and avoid the onset of noninvertible features on the predictions of ANNs.

2. The neural network configuration

In the examples to be presented, we made use of a 'standard' neural network configuration consisting of four layers (see Fig. 1), including two nonlinear hidden layers (of equal size) with the customary sigmoidal activation function $[g(y) = 1/2(1 + \tanh(y))]$. This configuration has been established as a good choice for black-box identification of nonlinear systems (see e.g. Lapedes & Farber, 1987) through the construction of discrete approximations of the type

$$\vec{X}(t+\tau) = F(\vec{X}(t), \vec{X}(t-\tau), \ldots; \vec{\gamma}) \quad (4)$$

where $\vec{\gamma}$ is the vector of operating parameters, $\vec{X}$ is the vector of states and τ is the delay. The vector of inputs is then the vector of states at the current time interval (and possibly at some previous time intervals) along with the (one or more) operating parameters. Similarly, the output layer gives the prediction of the vector of states at the next time interval. Both input and output layers are linear. Posing the identification problem in this particular way is common practice on the identifi-

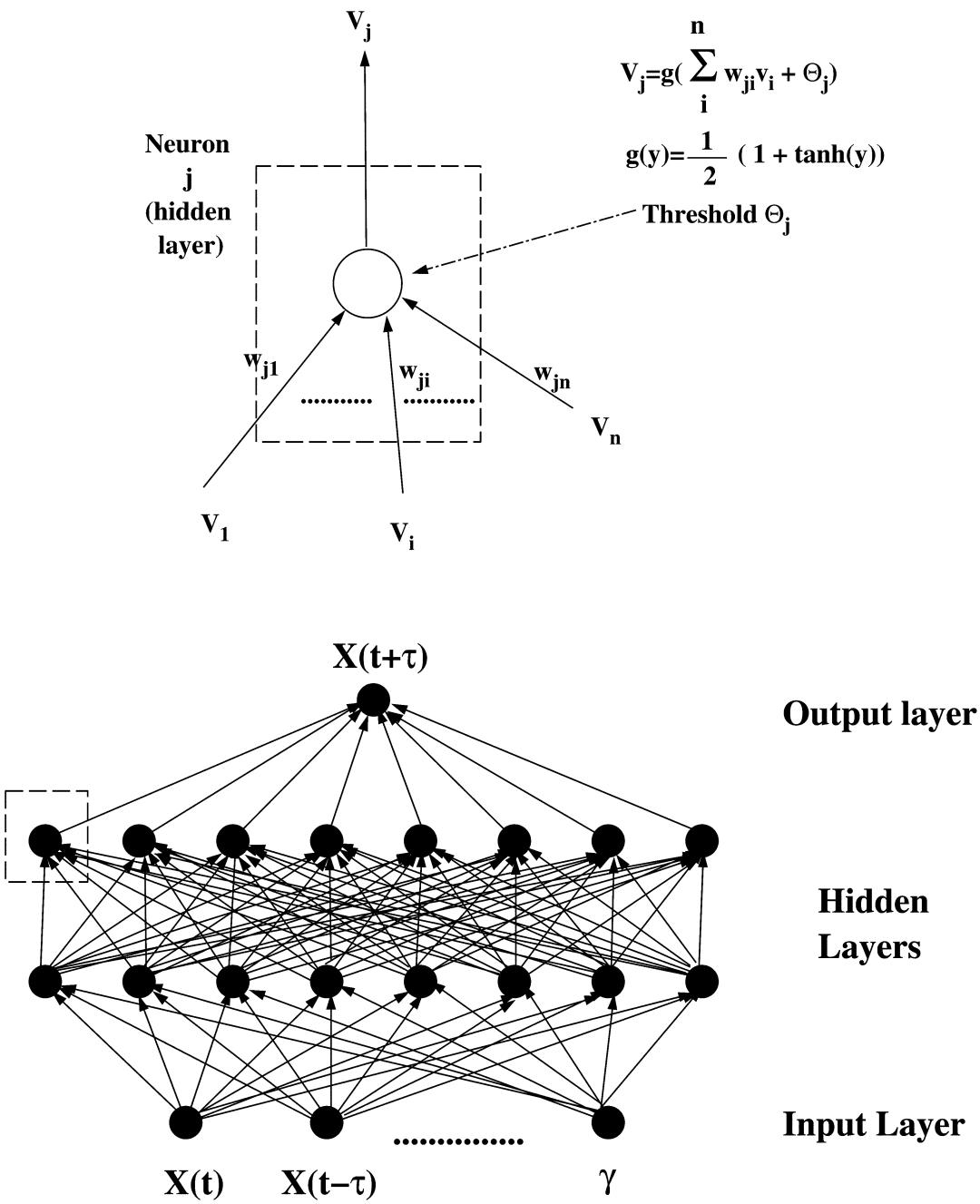

Fig. 1. Schematic of the neural network conguration used. The future state of the system $X(t+\tau)$ is predicted using the current value of the state, one (or more) 'delayed' values ($X(t)$, $X(t+\tau)$, etc.) and the parameter (γ).

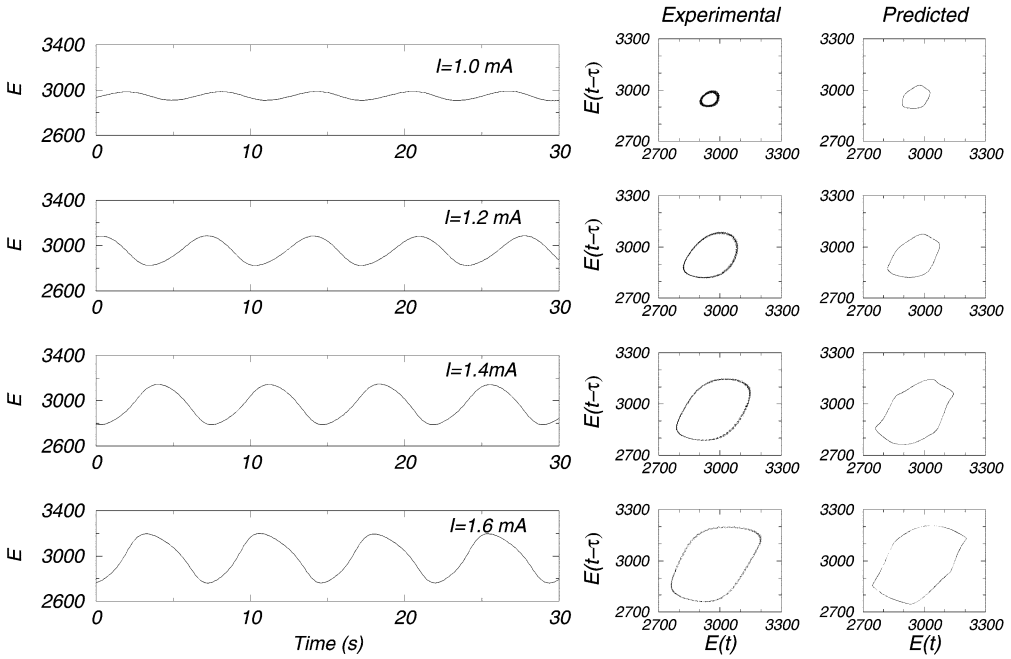

Fig. 2. Experimental time series, first column, and attractors, second column, from the electrochemical oxidation of hydrogen on a platinum anode under galvanostatic conditions. Each time series was collected at a different value of the applied current, noted in the figure. The variable plotted is a scaled version of the potential (to convert to millivolts divide by ten and add one hundred). In the third column the predicted attractors are shown. These phase portraits include the one included in the test set ($I = 1.4$ mA).

cation of systems using neural networks (see e.g. Lapedes & Farber, 1987; Bhat, Minderman Jr., McAvoy & Wang, 1990; Chu, Shoureshi & Tenorio, 1990; Chen, Billings & Grant, 1990; Hudson, Kube, Adomaitis, Kevrekidis, Lapedes & Farber, 1990; Ydstie, 1990; Su & McAvoy, 1991; Hernández & Arkun, 1992; Langonnet, 1992; Nahas, Henson & Seborg, 1992; Rico-Martínez, Krischer, Kevrekidis, Kube & Hudson, 1992; Tsung & Cottrell, 1993). Although we concentrate our discussion on the architecture noted above, our arguments will hold qualitatively for other architectures and other nonlinear activation functions.

3. Case I. Empirical modeling of an electrochemical reaction

As an example of noninvertibility arising in the construction of discrete-time neural network dynamic models from experimental data, consider the empirical modeling of an electrochemical reaction from experimental time series. This example will show how noninvertible phenomena can arise in a case of practical interest for which a good first-principles model of the system is not available.

Fig. 2 shows a set of time series collected from the oxidation of hydrogen at a platinum anode in the presence of Cu^{2+} and Cl^{-} under galvanostatic conditions. The data was provided by courtesy of Dr Katharina Krischer of the Fritz-Haber-Institut of the Max-Planck-Gesellschaft in Berlin. The time series were collected at different values of the operating parameter (the applied current, I, discussed in the figure caption). Further details about the experiments can be found in (Krischer, 1990; Krischer, Luebke, Wolf, Eiswirth & Ertl, 1991).

The range of dynamic phenomena we attempt to capture through an empirical ANN model is similar in nature to the examples discussed in (Rico-Martínez et al., 1993, 1994a) (a steady state undergoing a Hopf bifurcation). This case, however, is slightly different since the data are in the form of a single variable time series (as opposed to time series for all elements of the state vector). Following ideas common to system identification (the so-called ARMA models (Goodwin & Sin, 1984)) and methods used to reconstruct phase-space behavior of nonlinear dynamical systems (Packard, Crutchfield, Farmer & Shaw, 1980; Takens, 1981), we attempt to construct a mapping of the following form:

$$E(t+\tau) = F(E(t), E(t-\tau); I) \tag{5}$$

The function F will be approximated by a neural network. The *long-term behavior* prediction is obtained by iteration of this model: previous predictions of the neural network are fed back as inputs. $E(t)$ becomes

$E(t-\tau)$, $E(t+\tau)$ becomes $E(t)$, and thus the value of $E(t+2\tau)$ can be computed.

The neural network in this case contains eight neurons in each of the two hidden layers, and has one output ($E(t+\tau)$) and three inputs ($E(t)$, $E(t-\tau)$, and I). The time delay τ was chosen to be 1.25 s (about one fifth of the period of oscillation). The training set was constructed using 102 points from each of six times series taken at 0.975, 1.0, 1.05, 1.1, 1.2 and 1.6 mA, for a total of 612 training vectors. These training data included the initial transient to the final attractor (apparently an oscillation, or limit cycle, whose amplitude and period vary with the operating parameter I). A seventh experimental time series (at $I=1.4$ mA) was reserved to provide data for the test set. Training was performed using a conjugate gradient (CG) algorithm, and was considered complete after seven complete CG cycles (the average error was below 1.5%). The criterion to declare convergence included additional training for ten more CG cycles without any significant improvement on the predictive capabilities of the network. It is important to note that the neural network was not trained to convergence. A stopping criterion based upon standard cross-validation techniques was used to ensure that the training was terminated for a minimum of the generalization error (as measured for the test set), and not for a minimum of the error with respect to the training set. Thus, the phenomena described below are not a result of over-fitting.

Fig. 2 compares also the experimental and observed long-term attractors, including the parameter value corresponding to the test set. Let us emphasize that this is not the short-term, one-step-ahead prediction, but the long-term attractors of the two systems. *Any* initial condition in the general neighborhood of these attractors will give rise to transients eventually attracted to them. What for the system (and its unknown ODE model) is a *stable limit cycle* becomes a *stable (attracting) invariant circle* for the discrete-time neural network map. The location of the long-term attractors and their 'appearance' seem to indicate that the neural network succeeds in capturing all the features of the system, including the Hopf bifurcation predicted at 0.83 mA (compared with the experimental value of approximately 0.95 mA). While the iterated prediction in time inevitably deteriorates, and the real and predicted time series do not necessarily match point by point after a sufficiently long period of time, the *attractors* of the two dynamical systems *as sets in phase space* lie close to each other forever. This means that the *qualitative* dynamics are accurately reproduced. Note that time series at parameter values before the Hopf bifurcation point were not available; thus the poor prediction of the location of the bifurcation can be attributed to the lack of training data in this region of the parameter range.

3.1. Pathology I: J_n curves and multiple preimages

In Fig. 2, we see that the predicted attractors 'visually' appear to faithfully reproduce the experimentally observed data. However, there are features 'hidden' in the phase space which play an important role in the structure and bifurcations of the attractors as I varies. These features are important for determining when interpolations/extrapolations of the empirical ANN model predictions to other parameter values can be considered admissible. This onset of inadmissibility is signaled by curves in phase space defined by the vanishing of the determinant of the linearization of the forward-time mapping — locations where at least one eigenvalue of the linearization is zero. These hypersurfaces of codimension-1 (curves in a two-dimensional phase space) are called J_0 curves (surfaces) in the noninvertible map literature (Gumowski & Mira, 1980; Mira, 1987; Frouzakis, Gardini, Kevrekidis, Millerioux & Mira, 1997). Recently the terms LC (from the French 'ligne critique') for J_1 and LC_{-1} for J_0 have also been used (Gardini, 1991). Along with their nth iterations (J_n curves), these *critical* curves play a crucial role in generating noninvertible dynamical features, features not possible in the original data set. These critical curves undergo complicated sequences of transitions themselves as the operating parameter I varies, affecting the global dynamical behavior.

Following the ideas illustrated in (Rico-Martínez et al., 1993, 1994a) we construct the critical curves (J_n) numerically; in our examples the phase space is two-dimensional and so these are indeed curves. Working in two phase space dimensions makes both the presentation and the understanding of the concepts and the phenomenology much more tractable. The J_0 curves are defined by the points where the determinant of the 2×2 Jacobian matrix (the linearization) of Eq. (6) around $(x_n,y_n)\equiv(E(t),E(t-\tau))$ vanishes

$$x_{n+1}=F(x_n,y_n;I)$$
$$y_{n+1}=x_n. \tag{6}$$

When iterating forward in time, the phase space is 'folded' along the J_0 curves and mapped 'within' itself (the ANN map is an *endomorphism*). The image, J_1, of the J_0 curve constitutes then (after folding and mapping) the edge of a region whose points possess *more than one* preimage; it can be constructed by iterating once, forward in time, points on the J_0 curve (Gumowski & Mira, 1980; Mira, 1987; Frouzakis et al., 1997). Fig. 3 shows the ANN-predicted invariant circle for $I=1.1$ mA and $I=1.6$ mA (in the training range) along with the nearby J_0 and J_1 curves — more precisely, J_0 and J_1 sets, consisting each of several branches — computed for the converged ANN map. At the lower parameter value we observe a J_0 curve

branch *very close* to the actual attractor, along with its associated J_1 curve (the image of this particular J_0 branch). For each point on the attractor, there exists a 'relevant' preimage *on the attractor itself*. In addition to the 'relevant' preimage (the attractor itself), two *excess* preimages of the attractor were identified in this parameter range: one to the right, partially shown in Fig. 3(a), the other far to the left outside the range of the plot. Since no explicit expression for the inverse mapping of Eq. (5) is available, the preimages are computed using a nonlinear numerical solver (such as a Newton–Raphson iteration). Also, given the transcendental form of the constructed approximations, there is neither a practical way to compute all the 'roots' of the inverse mapping, nor even a means of determining how many exist. The following discussion is based on calculations limited to a finite neighborhood of the attractor in phase space (which we refer to as 'the relevant region'). The critical curves (J_n) themselves are computed numerically using a nonlinear equation solver and continuation techniques (Doedel, 1981).

As the parameter I is increased, the nearby J_0 curve branch 'drifts away' from the attractor. Fig. 3(b) shows the attractor and nearby critical curves at $I = 1.6$ mA. Although the attractor shows some 'pointy' features (compared to what one would visually expect from a limit cycle), they cannot be attributed to noninvertibility since there is no apparent interaction of the critical curves with the attractor at this parameter value. The attractor predicted by the network exhibits only one preimage in the relevant region (on the attractor itself). Thus, it appears that, at least for the parameter range used for training, the predicted attractor is free of noninvertible features.

This situation changes drastically as we probe the predictive capabilities of the network, extrapolating and exploring beyond the parameter range used in training. A new isolated J_0 curve branch appears in the vicinity of the attractor around $I = 1.6302$.

As the parameter is increased, the new-born J_0 curve, and its iterate J_1, grow. The lower part of the lense-like J_1 curve eventually crosses the attractor. This crossing can be seen to result in the 'birth' of a new preimage of the attractor in the vicinity of the J_0 isola. Only a short segment of the attractor has points with more than one preimage; the excess, non-physical meaningful ones lie on this new preimage curve. Fig. 4 shows the attractor along with its new excess preimage and the critical curves for $I = 1.65$ mA. The crossing of the J_1 curve with the attractor can be better visualized in the blowup Fig. 4(c).

As the parameter is further increased the newborn excess preimage curve grows and approaches the attractor. They touch at the same parameter value that the J_0 isola becomes tangent to the attractor. At this parameter value (around $I = 1.7$ mA), the upper part of the lense-like J_1 isola becomes tangent to the attractor at the (forward) iterate of its point of tangency with the J_0 isola. The point of tangency of the attractor with the J_1 curve has a special 'quartic' character, due to its marking the birth of the two 'quadratic' tangencies of the attractor and the J_1 curve. These are associated with the attractor crossing the J_0 curve in two places. A more detailed discussion of how a one-dimensional attractor (a curve in the neighborhood of its intersection with J_0) gives rise to the quadratic tangency with the corresponding J_1 branch is given in (Frouzakis, 1992; Frouzakis et al., 1997).

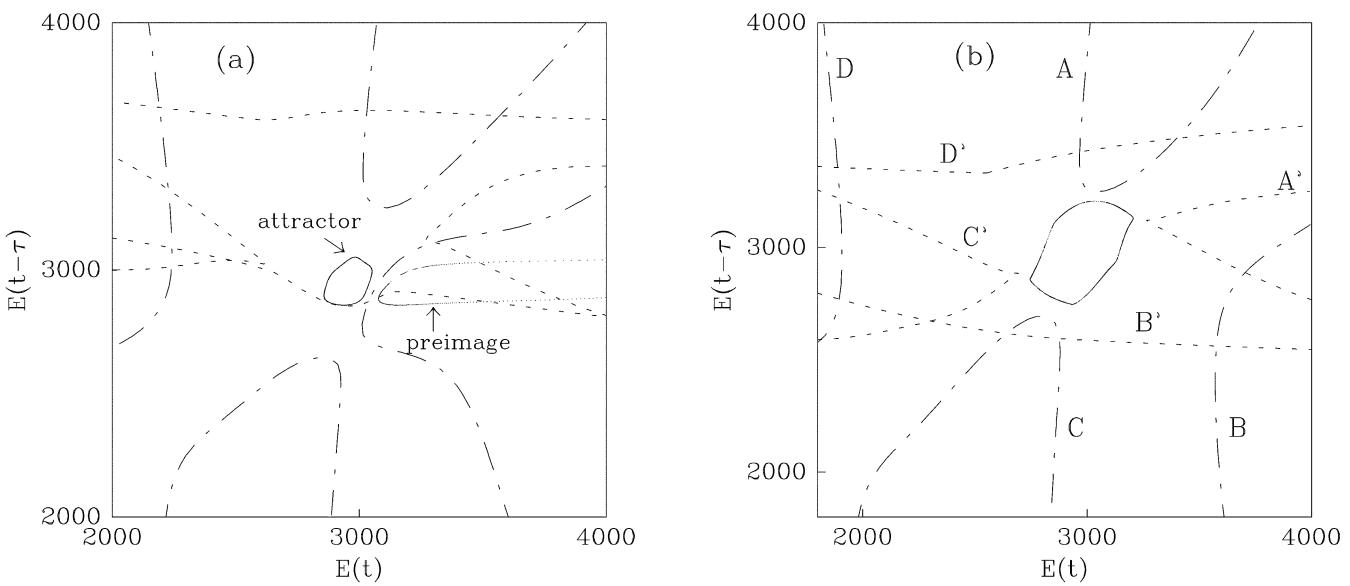

Fig. 3. Predicted attractors and critical curve sets for two different parameter values: $I = 1.1$ mA (a) and $I = 1.6$ mA (b). The dash–dot curves (A–D) represent J_0 curve branches and the short dash (A′–D′) the corresponding J_1 curve branches.

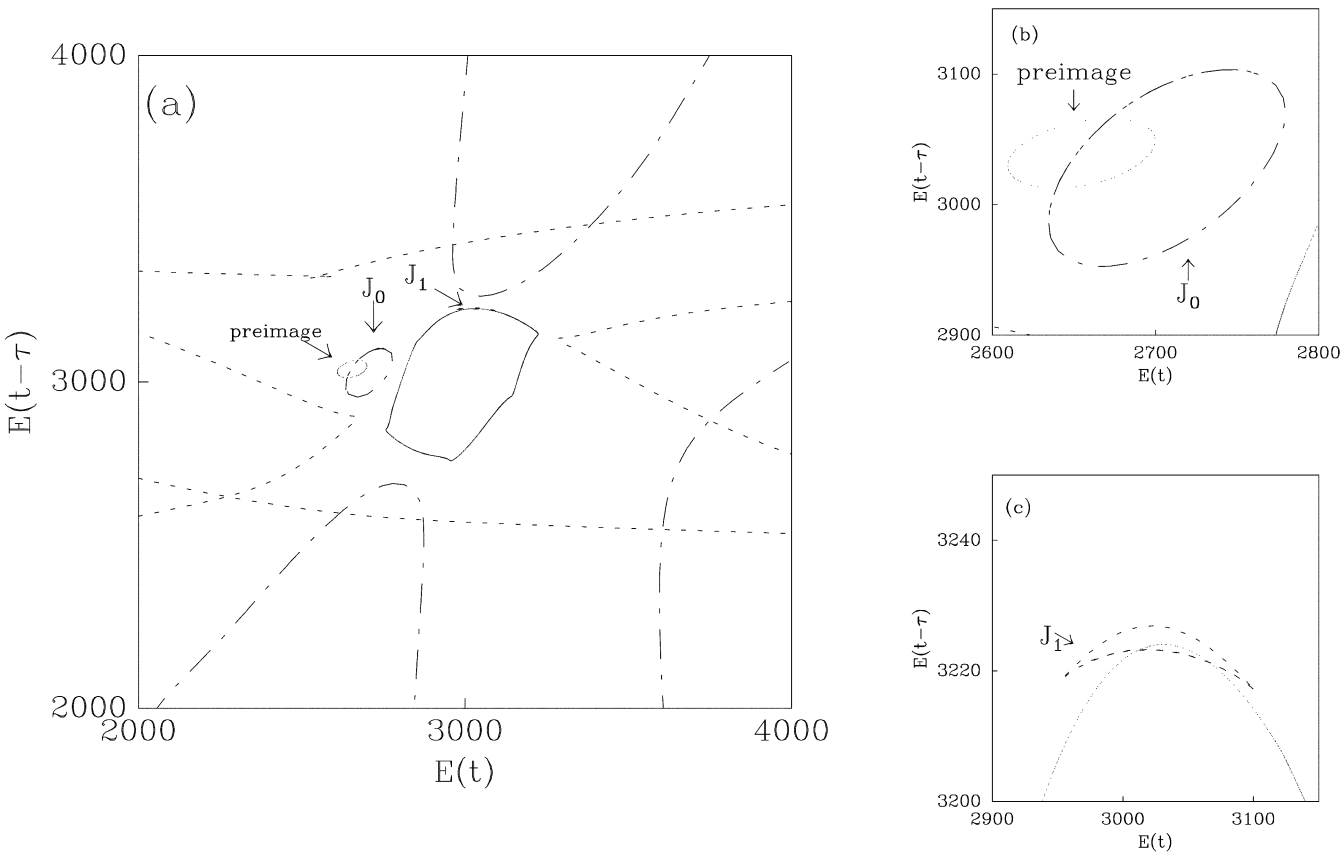

Fig. 4. The predicted attractor and critical curves for $I = 1.65$ mA. The lense-shaped J_1 curve crosses the attractor (see blowup in (c)), and so an additional excess preimage branch is formed, enlarged in (b) in the vicinity of the J_0 isola.

3.2. Pathology II: distorted attractors

If, in a predicted phase portrait, the attractor crosses a (computed) J_0 curve the dynamical behavior is 'visibly' noninvertible and pathological: successive iterations of a two-dimensional *invertible* system cannot jump first into and then out of the interior of an invariant circle (which represents the discrete-time form of a limit cycle in the plane) as happens now. In our example, at $I = 1.72$ mA some of the points on the attractor have excess preimages 'inside' and 'outside' the attractor in addition to the regular preimage 'on' the attractor. The intermingling of the new excess preimages and the attractor eventually distorts the 'round' shape of the attractor, as is evident in Fig. 5. This is one of the visible effects of the noninvertible character of the neural network approximation.

When searching for reasons to explain the appearance of noninvertible phenomena, it is tempting to 'blame' the noninvertible features of this network on the noise present in the experimental data. However, as we will illustrate in the example below, even when noise free (invertible) simulated data are used to train a neural network, it may predict attractors marred by noninvertible features.

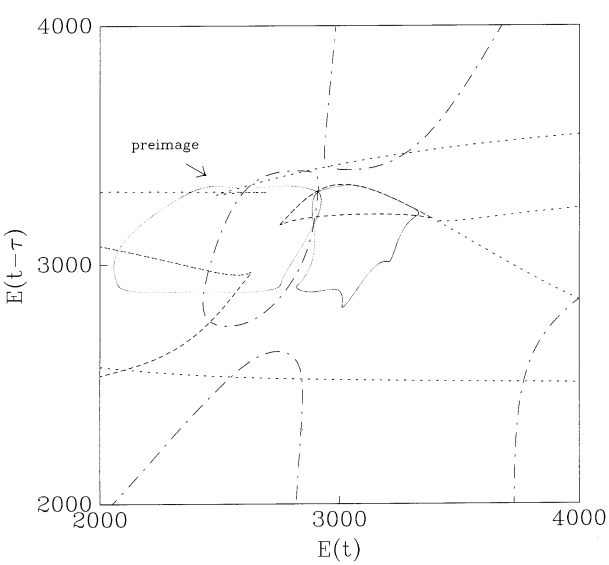

Fig. 5. The predicted attractor and critical curves at $I = 1.9$ mA. Note the distorted shape of the attractor.

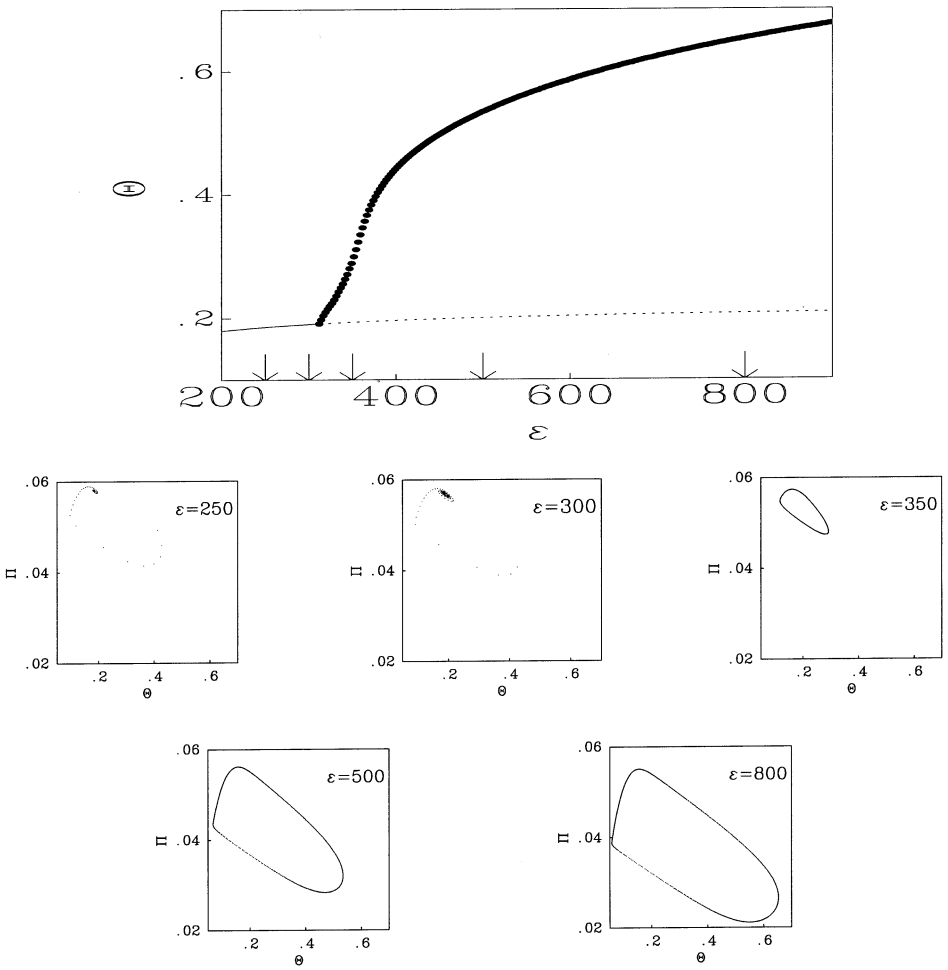

Fig. 6. Bifurcation diagram for the single species surface reaction system with respect to the parameter ϵ. Other parameters are fixed and given in the text. The arrows along the ϵ axis indicate where data points were collected for the training set and the phase portraits in the bottom show the attractors for these values. For $\epsilon = 250$ and 300, a transient approaching the attracting steady state is shown.

4. Case II. Surface reaction data

This example makes use solely of noise-free, uniquely invertible data to illustrate that noninvertibility can arise even when approximations of uniquely invertible deterministic time series are attempted using NN models. The data are obtained by integrating the following pair of ODEs describing a single species surface reaction (Kevrekidis, Schmidt & Aris, 1984):

$$\frac{d\theta}{dt} = \varepsilon[\Pi(1-\theta) - \theta e^{-\alpha\theta}] - s\theta$$

$$\frac{d\Pi}{dt} = \Pi_0 - \Pi + \varepsilon\Pi^*[\theta e^{-\alpha\theta} - \Pi(1-\theta)] \quad (7)$$

Here θ represents the reacting species coverage of the surface of the catalyst and Π is the dimensionless gas-phase pressure, i.e. a measure of the concentration of the reactant in the gas phase above the catalyst. The parameters $\varepsilon,\Pi_0,s,\alpha$, and Π^* are dimensionless groups of physical quantities. Further details about the system can be found in (Kevrekidis et al., 1984).

The training set was constructed by integrating Eq. (7) over a range of parameter values. Only a single parameter (ε) was varied in the neighborhood of a supercritical Hopf bifurcation point (in the range [250,800]), while the others were kept constant at $\Pi_0 = 0.11$, $s = 7$, $\alpha = 8$, and $\Pi^* = 0.04$. In this parameter range, the system exhibits (at low values of ε) a steady state that undergoes a Hopf bifurcation as ε is increased. Fig. 6 shows the numerically computed bifurcation diagram for this system; the arrows indicate parameter values at which data were collected for the training set. The insets at the bottom of Fig. 6 show the phase-space behavior of the system for each of these parameter values.

In order to guarantee that our training data are uniquely invertible backward in time, care was taken to perform the numerical integration of the pair of ODEs using an accurate backward difference 'stiff' integrator with error control (Leis & Kramer, 1988). The training set consisted of 340 points distributed over the five parameter values chosen: 20 points for $\varepsilon = 250$, 40

points for $\varepsilon = 300$, 80 points for $\varepsilon = 350$ and 100 points each for $\varepsilon = 500$ and $\varepsilon = 800$. The trajectories on which these points lie include initial transients approaching the attractors as well as data on the attractors themselves. Note that more points have been added to the training set at parameter values where more complicated long term behavior (larger amplitude oscillations) is observed; here, 'complicated' should be compared to parameter values where 'simpler' trajectories approaching a steady state are found.

4.1. The neural network

The mapping we seek to construct is of the form:

$$\theta(t+\tau) = F(\theta(t),\Pi(t);\varepsilon)$$

$$\Pi(t+\tau) = G(\theta(t),\Pi(t);\varepsilon)$$

where the functions F and G are approximated by the neural network. The delay τ was chosen to be 0.22 units of time (approximately one-fifth of the period of the oscillations). A four-layer neural network was used, consisting of eight neurons in each hidden layer, three inputs (ε, $\theta(t)$, and $\Pi(t)$), and two outputs ($\theta(t+\tau)$, and $\Pi(t+\tau)$). The results presented below were obtained after 170 complete conjugate gradient (CG) cycles, when the average norm error dropped below 1.5% of the available range in the training set. The criterion for stopping training involved using a test set consisting solely of points not in the training set. Training was continued over 100 more CG cycles without observing any appreciable improvement in predictions (nor any significant qualitative change of the noninvertible phenomena described below). Once again, the results reported are for a minimum on the generalization error as measured for the test set and not the result of over-fitting.

The resulting neural network faithfully predicts the behavior of the system at low ε values. At $\varepsilon = 290$, for example, Eq. (7) has a single stable steady state at $\theta = 0.1893$, and $\Pi = 0.0570$. At the same ε value, the network predicts a stable steady state at $\theta = 0.1863$, and $\Pi = 0.0571$. The network also predicts the Hopf bifurcation point location with reasonable accuracy (for Eq. (7) the Hopf bifurcation occurs at $\varepsilon = 311.8$ and it is predicted by the neural network at $\varepsilon = 318.65$). Close to the Hopf bifurcation, the predictions of the limit cycle oscillations are also good. In Fig. 7, the predicted phase space attractor is plotted next to the true attractor of Eq. (7). Note the appearance of visual 'corners' in the predicted attractor as compared to the smoother contour of the true attractor. As we will see, this is a prelude to the onset of noninvertible behavior.

4.2. Pathology III: resonant (frequency locked) solutions

The long-term predictive capabilities of the network deteriorate severely for larger values of the parameter ε. The role noninvertibility plays can be better understood by analyzing the behavior of the system prior to the predicted Hopf bifurcation in a similar manner as it was done for the previous example. The resulting effect of the noninvertible character of the map is very similar to the one described before; however, the noninvertible phenomena leading to it are drastically different. A detailed description of these events is beyond the scope of the discussion presented in this paper. We will concentrate on the description of the most evident pathologies that result from the noninvertible character of the neural network mapping: those that may aid the neural network practitioner in identifying the effects of noninvertibility on the validity of the predictions exhibited by an ANN.

After the Hopf bifurcation, and as the operating parameter is increased, the predicted invariant circle grows in amplitude. Fig. 8 shows a sequence of phase portraits depicting the attractor and its interaction with its excess preimages as ε is increased from 325 to 342.

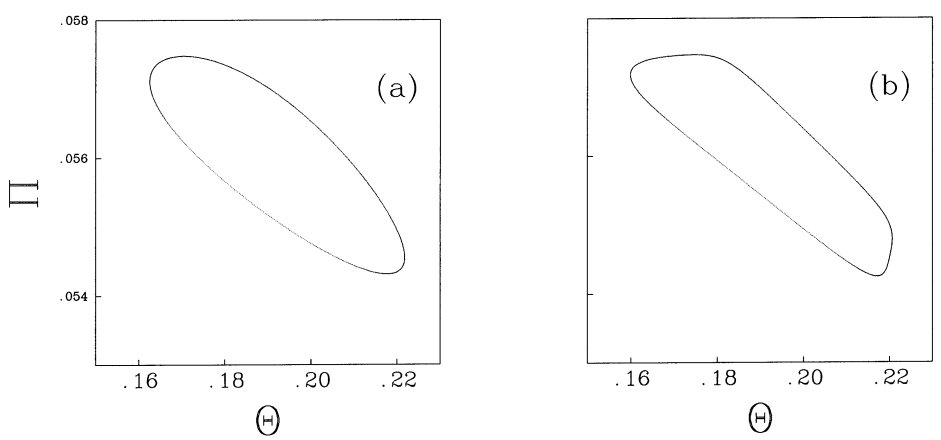

Fig. 7. Actual (a) and predicted (b) attractors for the single species surface reaction example for $\epsilon = 321$.

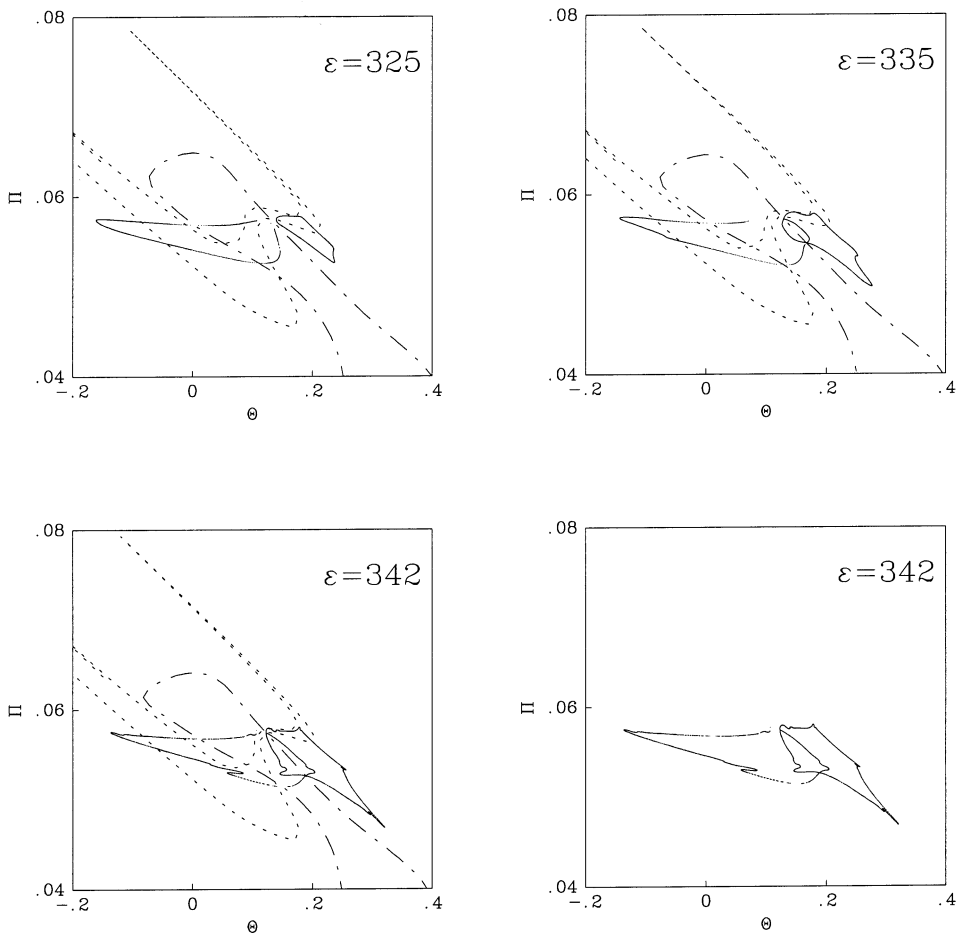

Fig. 8. The growth of the predicted invariant circle and its interaction with its preimages and critical curves as ϵ is increased. The 'smooth' invariant circle crosses the nearby J_0 curve, interacts with its preimages, and acquires an increasingly distorted shape.

The sequence in Fig. 8 is very similar to the one observed for the noninvertible map of the previous example, based on modeling experimental data from the electrochemical oxidation of H_2. The invariant circle grows, hits a nearby J_0 curve, and subsequently overlaps with one of its excess preimages — we see that, in this example, clear indicators of noninvertible dynamical behavior appear *within* the parameter range used for training the ANN. As this interaction becomes more intense, the attractor grows increasingly distorted. At $\varepsilon = 342$, however, we still can qualify the attractor as a smooth C^∞ invariant circle. Although the attractor exhibits some 'wiggles', there is no evidence of the attractor *intersecting itself*.

As we continue to increase the parameter ε value, the predicted dynamical behavior changes qualitatively through a combination of both noninvertible and nonlinear, *invertible* mechanisms. In Fig. 9, we observe a saddle-node bifurcation of period-5 fixed points occurring *on* the predicted invariant circle at $\varepsilon = 344.5$. These *resonant*, or *frequency-locked* solutions are born as the ratio of the oscillation and sampling frequencies changes from an irrational to a rational number. In this case, the sampling frequency is five times the frequency of the overall oscillation. These resonant solutions persist to $\varepsilon = 384.16$, where both the period-5 saddle and node are destroyed in another saddle-node bifurcation.

Within this interval of existence of period-5 solutions, the attracting nodes undergo a period-doubling bifurcation (see Fig. 9), which initiates a cascade of period-doubling bifurcations. This gives rise to a complicated, apparently chaotic attractor, which eventually collapses back to a period-5 node through a reverse sequence of period-'halving' bifurcations. Interspersed with these bifurcations of the attractor, there occur several *global* bifurcations involving the unstable manifolds of the saddle-type period-5 solutions. These bifurcations, *while also displayed by invertible dynamical systems*, are rendered immensely more complicated by the noninvertible nature of the neural network. It is precisely the interplay of these two mechanisms which is responsible for the deterioration of the quality of the long-term network predictions.

To analyze the global bifurcations responsible for the loss of smoothness of the invariant circle (from behavior A to C of Fig. 9), we reconstruct the invariant circle by computing the unstable manifolds of the saddle-type period-5 solutions (which we refer to here as the 'saddle-unstable manifolds'). Since we wish only to illustrate some of the possible dynamic phenomenology, and not delve into the theory of the observed bifurcations, we briefly note that the definition of global stable and unstable manifolds valid for invertible mappings does not directly hold for noninvertible ones and must be modified. Nevertheless, it is possible to define local versions of both stable and unstable manifolds, as well as a global *unstable* manifold (Robinson, 1994; Frouzakis et al., 1997). Fig. 10 shows the result of one such calculation: a wiggly, but still smooth circle connecting the saddle period-5 points and the period-5 nodes. However, we see from Fig. 10 that this structure crosses one J_0 and one J_1 curve and so we should suspect that noninvertibility will come into play during the bifurcations and transitions which will occur for larger ε.

4.3. Pathology IV: global bifurcations and self-intersecting attractors

The presence of 'wiggles' in the saddle-unstable manifold in the neighborhood of the period-5 node of Fig. 10 indicates the onset of a global bifurcation. This global bifurcation involves the crossing of the unstable manifold of the period-5 saddle with the (local) strong stable manifold of the period-5 node. Fig. 11 consists of snapshots of the different stages of this transition. At $\varepsilon = 345$, just after the period-5 frequency locking, the wiggly unstable manifold is still far from the (local) strong stable manifold of the node-period-5, but approaches it and eventually crosses it at approximately $\varepsilon = 347$. The node period-5 solutions are born with one negative eigenvalue. This means that iterations along the strong stable eigendirection alternate from one side of the (strong stable eigenvector of the) node to the other, and so the saddle-unstable manifold also has to switch back and forth as it asymptotes to the node for

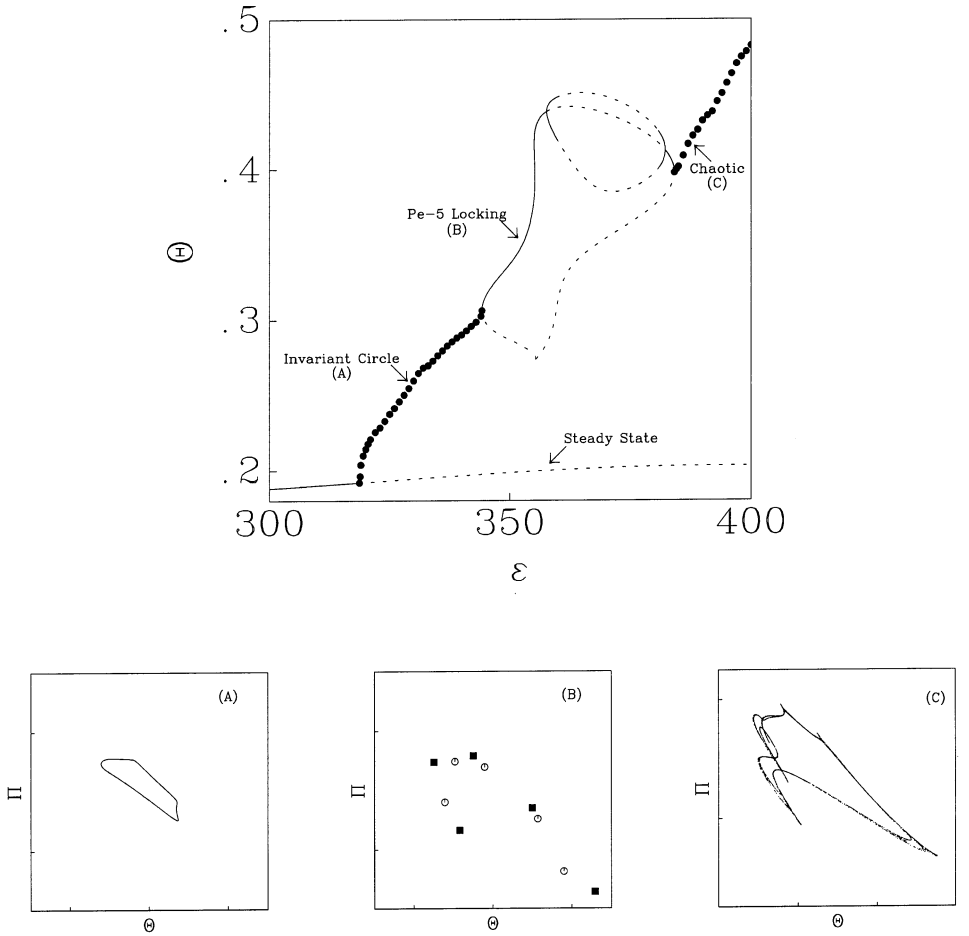

Fig. 9. A portion of the bifurcation diagram predicted by the neural network mapping constructed using simulated data for the surface reaction model. Stable fixed points are indicated by solid curves, unstable fixed points by broken curves and invariant circles (A) by filled circles. The branch of period-5 periodic points (B) resulting from a resonance (frequency-locking) on the invariant circle is indicated in the plot. This branch undergoes a sequence of period doubling bifurcations, of which only one is included in the diagram. After the disappearance of the locked states the resulting attractor (C) appears chaotic.

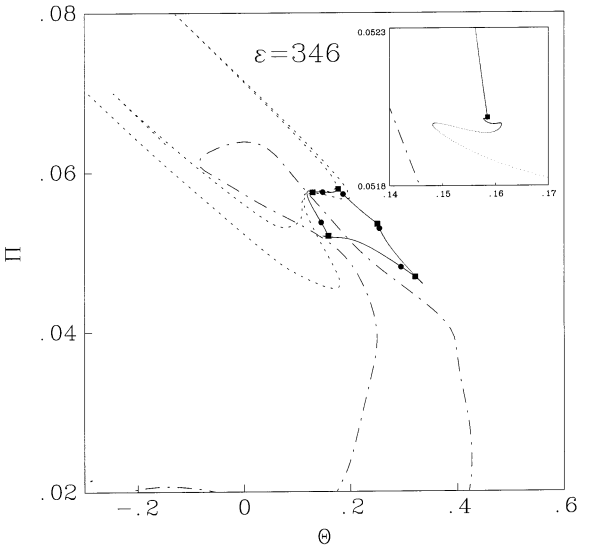

Fig. 10. Predicted closed invariant curve constructed using the unstable manifolds of the period-5 saddles at $\epsilon = 346$, superposed on the critical curves. The saddle points are represented with circles and nodes with squares. The inset of the top shows the saddle-unstable manifolds approaching one of the period-5 stable nodes, which are the attractor at this parameter value.

parameter values in the neighborhood of this bifurcation.

Since global bifurcations take place over a region of phase space and a range of parameter values, the crossing still takes place at $\varepsilon = 348$. It can be seen in Fig. 12 that 'on its way' to the period-5 node, the saddle-unstable manifold also crosses the J_0 curve; for this specific parameter value, however, *at* the point of crossing with J_0, the saddle-unstable manifold happens to be tangent to the eigenvector e_0 associated with the zero eigenvalue of the linearized mapping. It can be shown (Frouzakis et al., 1997, and it is obvious in Fig. 12) that, at the iterate of this point, which by construction also lies on the global saddle-unstable manifold *and* on J_1, the saddle-unstable manifold develops a *cusp* (or kink). The net result is a loss of smoothness of the invariant circle, a clearly observable sign of the loss of validity of predictions made by the neural network. It is important to note, however, that the other 'side' of the saddle-unstable manifold remains unaffected: it asymptotically approaches another period-5 node along its weak local stable manifold while this bifurcation occurs.

As ε is increased, the cusps 'open' into self crossing *loops* of the saddle-unstable manifold. Another important manifestation of noninvertibility is that the negative eigenvalue of the node crosses zero, and so the node changes from orientation-reversing to orientation-preserving. The implication of this transition is that the self-crossing loops no longer switch back and forth near the node, but asymptotically approach it in a monotonic, spiraling fashion. The self-crossing loops appear to reform into kinks as ε is increased to a value of 351: the events leading to the formation of the self-intersections are reversed. The eventual outcome of this sequence of transitions is an invariant circle which is relatively smooth, without any evident noninvertible features that would signal invalid predictions by the neural network model.

A second global bifurcation takes place at about $\varepsilon = 352.55$. This time the bifurcation involves the *other* side of the saddle-unstable manifold (the one not involved in the first global bifurcation). As before, the saddle-unstable manifold develops wiggles for a (very) small parameter range. This global bifurcation, however, does not seem to be accompanied by the development of self-crossings and other noninvertible features and its only result is that now both saddle-unstable manifolds approach the node from the *same* side of its (local) strong stable manifold.

The period-5 node begins a sequence of period-doubling bifurcations at approximately $\varepsilon = 357$. These ultimately result in a five-piece, apparently chaotic attractor (see Fig. 13(a)). The period-doubling cascade subsequently reverses itself, finally resulting in a stable period-5 node which exists for a small parameter range. In our simulations we did not detect any evidence of other attractors coexisting with the period-5 solutions. The period-5 solutions (saddle points and nodes) eventually annihilate each other in saddle-node pairs at $\varepsilon \approx 384.16$. On the 'other' side of this saddle-node bifurcation, we observe an (initially intermittent, or 'bursting') chaotic attractor which, as we will see, clearly possesses noninvertible features. What proves to be the important factor in the development of this chaotic attractor, which remains after the 'closing' the frequency-locked period-5 isola, is not the period-doubling cascade, but a sequence of global bifurcations.

Computing the saddle-unstable manifolds for $\varepsilon = 361$ (Fig. 13(b)) shows that in addition to approaching the node from the same 'side' of its (local) strong stable manifold, this arrangement has evolved into a 'braided' structure. In this 'braid', the saddle-unstable manifolds of *different* saddle points intersect, and so this can be considered a *heteroclinic* interaction. Fig. 14 shows the attractor just after the saddle-node bifurcation ($\varepsilon =$ 386). The attractor exhibits very evident self-crossings and is clearly noninvertible in nature. These can be thought as 'echoes' or remnants of the self-intersections of the saddle-unstable manifolds, when the saddles still existed, before the saddle-node bifurcation.

Our brief description of the observed phenomena was not intended to be exhaustive or comprehensive. It was also not meant to be a survey or self-contained introduction to noninvertible global bifurcations for readers

not familiar with the phenomenology of noninvertible mappings, or even with global bifurcations of invertible mappings of the plane. For readers not familiar with this terminology and phenomena we hope that this serves as a brief anthology, and as an indication of the richness and complexity of the types of noninvertible dynamics that can be predicted by NN models. Clearly, even if the predicted time series appear 'reasonable', phase space plots exhibiting such phenomena invalidate the NN models.

5. Discussion

In this paper, we discussed an inherent deficiency of ANN-based discrete-time nonlinear models obtained from time series. This deficiency, noninvertibility, provides also an alternative method for judging the validity of predictions made by the ANN models. This idea differs from what might be considered the 'traditional' methods for assessing the predictive capabilities of the ANN models, such as validation with test data not

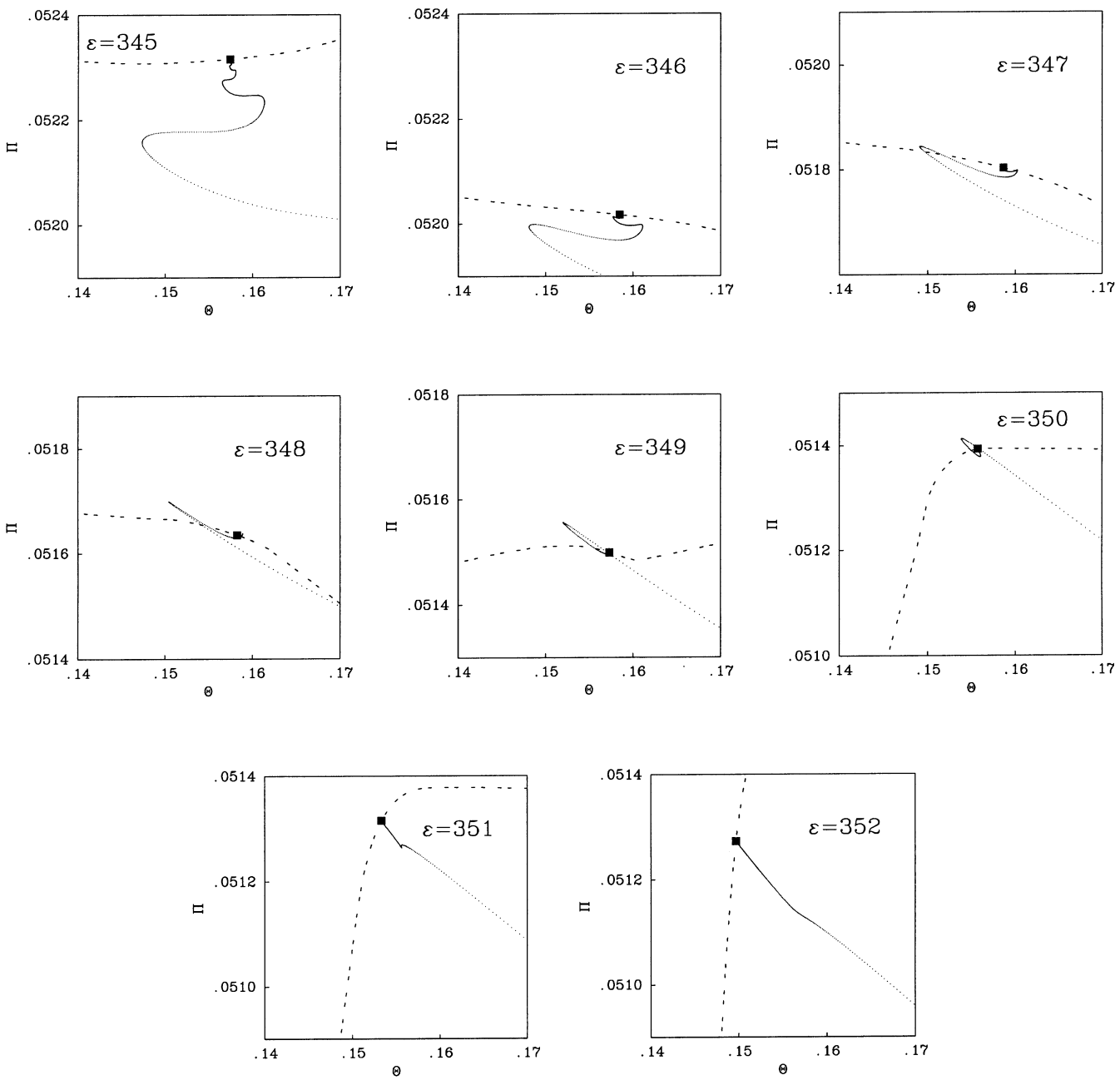

Fig. 11. A sequence of blowups of one of the period-5 nodes born from the locking on the invariant circle, illustrating the global bifurcation involving the unstable manifold of the saddle period-5 and the node's strong stable manifold (double-dash curve). Note that the 'wiggling' of the unstable manifold increases as it approaches (in parameter space) the crossing with the strong stable manifold. The unstable manifold also develops self-intersections as a result of its interaction with the critical curves.

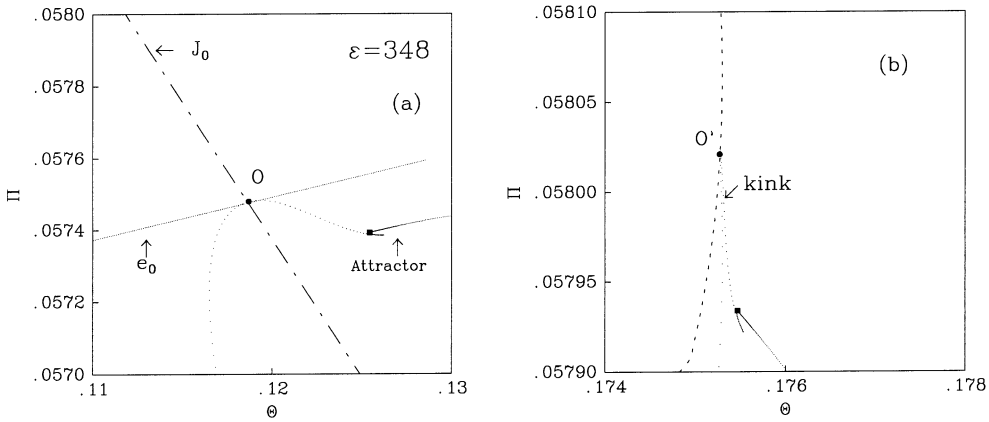

Fig. 12. Enlargement of one of the panels of Fig. 11 in the neighborhood of the period-5 node, showing the e_0 tangency responsible for the kink and subsequent self-crossing of the unstable manifold.

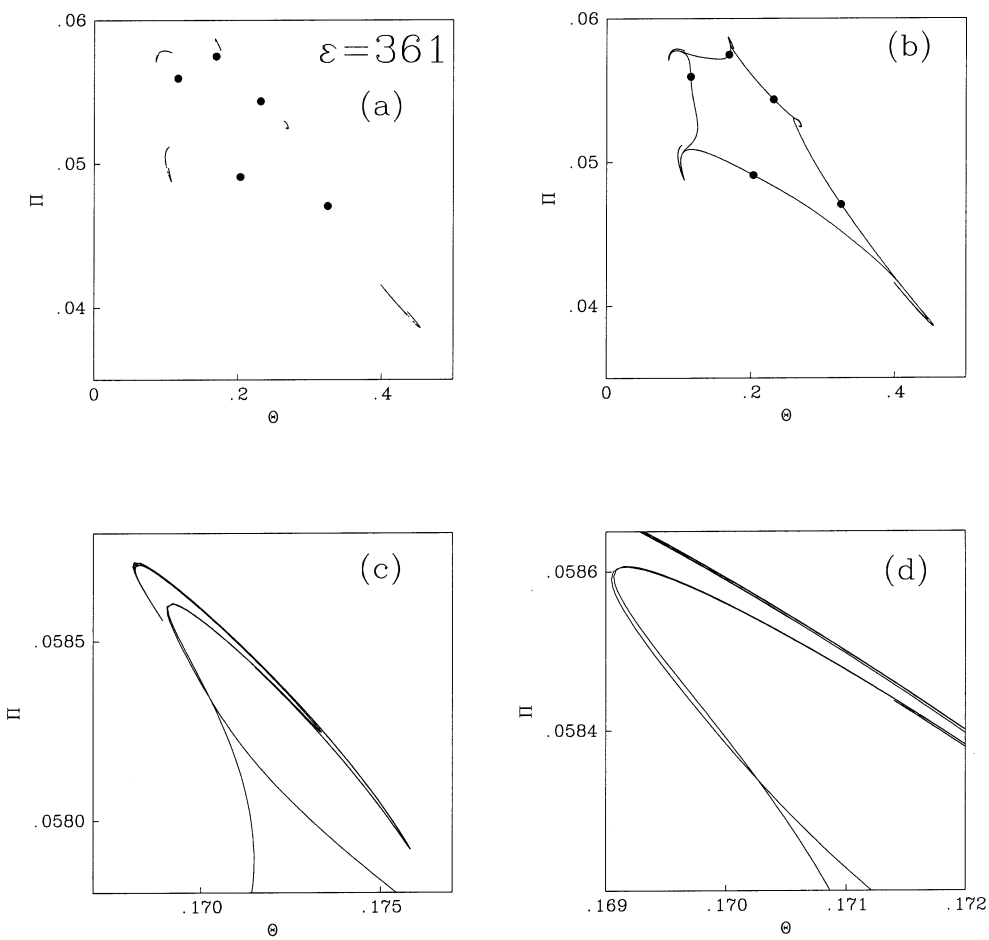

Fig. 13. The five-piece attractor (a), saddle-unstable manifolds asymptotically approaching it (b), and enlargements of the 'braiding' structure of the manifolds (c) and (d) for $\epsilon = 361$.

included in the training set. This criterion is based on the 'post-mortem' searching for qualitative features in the long-term model predictions which are impossible in the original system. By presenting a study of the noninvertible dynamical behavior of neural network models trained on invertible data, we uncovered mechanisms responsible for the deterioration of the predictive capabilities of the model. While details of the bifurcations and transition sequences discussed are specific to the systems studied, the basic building blocks of *critical curves in phase space* are generic features of noninvertible systems. This means that our strategy of construct-

ing critical curves and studying their interactions with the predicted attractors is applicable to other neural network models, provided that the dimension of the phase space is relatively low (≤ 3).

Adjustable factors such as the size and architecture of the neural network, the size and composition of the training set, the degree of training, and the magnitude of the delay can, and will, affect the particular manner in which noninvertible behavior appears. These choices, however, cannot alter the fundamentally noninvertible nature of the neural networks discussed in this paper — noninvertibility will appear in one way or another in this type of model. The best that can be done is to use the choices mentioned above to 'displace' the noninvertible phenomena *out of the relevant region of phase space*. For example, determining *where* in phase and parameter space the critical curves begin to interact with the predicted attractors can be used as a guideline for the acquisition of more training data to improve the predictions. Smaller time delays may also reduce noninvertible effects, although the increased correlation between points in the time series will work against more accurate predictions. It would be interesting to examine how one might include the distance of J_0 curves as a constraint in the training, and thus devise training algorithms that would guarantee the lack of spurious excess preimages in the relevant region of phase space.

Another interesting direction of research involves the use of pruning algorithms in order to diminish the effects of noninvertibility. In classification applications, the pruning of neural network often results in increasing smoothing of the decision boundaries (Reed, 1993). For noninvertible neural network predictors, pruning may result in the modification of the J curves interaction with the predicted attractors. However, the current pruning algorithms should be modified to consider the effect of eliminating connections on the *long-term* behavior of the NN model.

An alternative approach to eliminating noninvertible dynamical features is to avoid them completely from the outset. This can be accomplished by constructing input/output neural network mappings which approximate the *time derivatives* of the states at each time step (the right-hand-side of the system ODEs) (e.g. Chu &

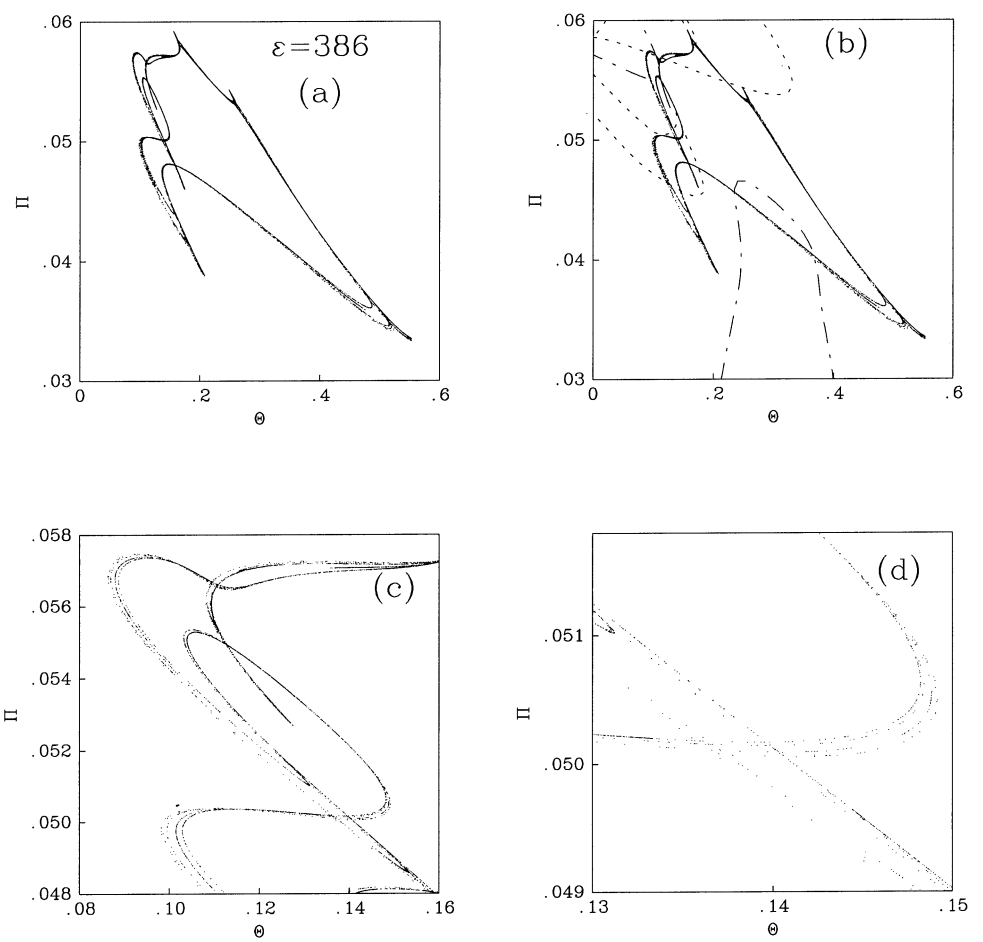

Fig. 14. The predicted chaotic attractor (a), superposed with its neighboring critical curves (b) at $\epsilon = 386$, just after the saddle-node bifurcation. The predicted, apparently chaotic, attractor is characterized by self-intersections (see the enlargements in (c) and (d)), clearly indicating its noninvertible nature.

Shoureshi, 1991; Rico-Martínez et al., 1992; Rico-Martínez, Anderson & Kevrekidis, 1994b; Rico-Martínez et al., 1995; Rico-Martínez & Kevrekidis, 1993; Olurotimi, 1994). We thus construct *continuous time models*, and then using an accurate numerical integrator, follow the time evolution of the system, rather than predict the state at the next (fixed) time step directly. 'Perfect' integration is by construction uniquely invertible: trajectories, given the appropriate conditions on the right-hand-side, are unique in reverse time. A numerically accurate integration between two points in a time series would guarantee that the excess preimages (also always present in numerical integration schemes (Lorenz, 1989)) will not interfere with the local dynamics.

From the examples presented here, it is clear that noninvertibility plays a very important role in the deterioration of the predictive capabilities of discrete neural network approximations of continuous-time nonlinear dynamical systems. The numerical computation of *critical curves* in phase space, on the other hand, can be used as a tool to assess the validity range of ANN predictions. Although we have stressed the effect of noninvertibility on the long-term prediction capabilities of the ANN models, noninvertibility translates also in important local effects that may drastically affect the quality of the short-term predictions over a limited region of phase space (in the close vicinity of J_0 curves). For example, in discussing pathology IV we found a noninvertible transition that changes an attractor from orientation preserving to orientation reversing. Locally, this observation translates also in incorrect short-term predictions because it implies that the trajectories will go from the 'outside' to the 'inside' of the periodic orbit. While again this is a valid possibility for discrete noninvertible systems, it is simply impossible for continuous systems.

The study of noninvertible dynamical systems is an important and recently flourishing research subject in itself. Some of the phenomena described here have not yet been widely observed or reported in the literature. Multistable noninvertible dynamical systems can have disconnected and highly distorted basin of attraction boundaries (Adomaitis & Kevrekidis, 1991). An interesting research problem might be the study of basin boundary structures of neural network models trained on data obtained from multistable, *invertible* systems to determine the role of noninvertibility in the breakdown of predictions of these systems. Finally, it is important to consider the implications of noninvertibility in neural network model-based feedback control systems, especially in terms of the complexity noninvertibility introduces into assessing the global stability of such systems.

Acknowledgements

The authors would like to acknowledge the support of the National Science Foundation and UTRC. One of the authors (R.R.M.) was partially supported by CONACyT; the hospitality of the Center for Nonlinear Studies at the Los Alamos National Laboratory is gratefully acknowledged.

References

Adomaitis, R. A., & Kevrekidis, I. G. (1991). Noninvertibility and the structure of basins of attraction of a model adaptive control system. *Journal of Nonlinear Science*, *1*, 95–105.

Bhat, N. V., Minderman Jr., P. A., McAvoy, T., & Wang, N. S. (1990). Modeling chemical process systems via neural computation. *IEEE Control Systems Magazine*, April, 24–29.

Chen, S., Billings, S. A., & Grant, P. M. (1990). Non-linear system identification using neural networks. *International Journal of Control*, *51*, 1191–1214.

Chu S. R., Shoureshi, R., & Tenorio, M. (1990). Neural networks for system identification. *IEEE Control Systems Magazine*, April, 31–35.

Chu, S. R., & Shoureshi, R. (1991). A neural network approach for identification of continuous-time nonlinear dynamic systems. *Proceedings of the* 1991 *American Control Conference*, *1*, 1–5.

Doedel, E. J. (1981). AUTO: a program for the automatic bifurcation analysis of autonomous systems. *Congressus Numerantium*, *30*, 265–284.

Frouzakis, C. E. (1992). Dynamics of systems under control: quantifying stability. *Ph.D. Thesis*, Princeton University, Department of Chemical Engineering.

Frouzakis, C. E., Gardini, L., Kevrekidis, I. G., Millerioux, G., & Mira, C. (1997). On some properties of invariant sets of two-dimensional non-invertible maps. *International Journal of Bifurcations and Chaos*, *7*, 1167–1194.

Gardini, L. (1991). On the global bifurcation of two-dimensional endomorphisms by use of critical lines. *Non Linear Analysis, Theory, Methods and Applications*, *18*, 361–399.

Gicquel, N., Anderson, J. S., & Kevrekidis, I. G. (1998). Noninvertibility and resonance in discrete-time neural networks for time series processing. *Physics Letters A*, *238*, 8–18.

Goodwin, G. C., & Sin, K. S. (1984). *Adaptive filtering, prediction and control*. Englewood Cliffs, NJ: Prentice Hall.

Gumowski, I., & Mira, C. (1980). *Recurrences and discrete dynamic systems*, Lecture Notes in Mathemathics, Springer, Heidelberg.

Hernández, E., & Arkun, Y. (1992). Study of the control-relevant properties of backpropagation neural network models of nonlinear dynamical systems. *Computers & Chemical Engineering*, *16*, 227–240.

Hudson, J. L., Kube, M., Adomaitis, R. A., Kevrekidis, I. G., Lapedes, A. S., & Farber, R. M. (1990). Nonlinear signal processing and system identification: applications to time series from electrochemical reactions. *Chemical Engineering Science*, *45*, 2075–2081.

Kevrekidis, I., Schmidt, L. D., & Aris, R. (1984). Rate multiplicity and oscillations in single species surface reactions. *Surface Science*, *137*, 151–166.

Kevrekidis, I. G., Rico-Martínez, R., Ecke, R. E., Lapedes, A. S., & Farber, R. M. (1994). Global bifurcation analysis in Rayleigh–Bénard convection experiments, empirical maps and numerical bifurcation analysis. *Physica D*, *71*, 342–362.

Krischer, K. (1990). Nichtlineare dynamik zweier grenzflächenreaktionen — Kinetische oszillationen, bifurkationen und deterministisches chaos. *Ph.D. Thesis*, Free University Berlin, Germany.

Krischer, K., Luebke, M., Wolf, W., Eiswirth, M., & Ertl, G. (1991). Chaos and interior crisis in an electrochemical reaction. *Berichte der Bunsengesellschaft fuer Physikalische Chemie*, *95*, 820–823.

Langonnet, P. (1992). Process control with neural networks: an example. *Applications of Artificial Neural Networks III*, SPIE 1709:468–475.

Lapedes, A. S., & Farber, R. M. (1987). Nonlinear signal processing using neural networks: prediction and system modeling, *Los Alamos Report LA-UR 87-2662*.

Leis, J. R., & Kramer, M. A. (1988). ODESSA — an ordinary differential equation solver with explicit simultaneous sensitivity analysis. *ACM Transactions on Mathemathics Software*, *14*, 61–67.

Lorenz, E. N. (1989). Computational chaos — a prelude to computational instability. *Physica D*, *35*, 299–317.

Mira, C. (1987). *Chaotic dynamics. From the one-dimensional endomorphism to the two-dimensional diffeomorphism*. Singapore: World Scientific.

Nahas, E. P., Henson, M. A., & Seborg, D. E. (1992). Nonlinear internal model control strategy for neural network models. *Computers & Chemical Engineering*, *16*, 1039–1057.

Packard, N. H., Crutchfield, J. P., Farmer, J. D., & Shaw, R. S. (1980). Geometry from a time series. *Physical Review Letters*, *45*, 712–716.

Olurotimi, O. (1994). Recurrent neural network training with feedforward complexity. *IEEE Transactions on Neural Networks*, *5*, 185–197.

Reed, R. (1993). Pruning algorithms — a survey. *IEEE Transactions Neural Networks*, *4*, 740–747.

Rico-Martínez, R., & Kevrekidis, I. G. (1993). Continuous-time modeling of nonlinear systems: a neural network approach. *Proceedings of the* 1993 *IEEE International Conference on Neural Networks*, *III*, 1522–1525.

Rico-Martínez, R., Krischer, K., Kevrekidis, I. G., Kube, M. C., & Hudson, J. L. (1992). Discrete- vs. continuous-time nonlinear signal processing of Cu electrodissolution data. *Chemical Engineering Communications*, *118*, 25–48.

Rico-Martínez, R., Kevrekidis, I. G., & Adomaitis, R. A. (1993). Noninvertibility in neural networks. *Proceedings of* 1993 *IEEE International Conference on Neural Networks*, *I*, 382–386.

Rico-Martínez, R., Kevrekidis. I. G., & Adomaitis, R. A. (1994a). Noninvertible dynamics in neural network models. *Proceedings of the Twenty-Eighth Annual Conference on Information Sciences and Systems* (pp. 965–969). Princeton, NJ: Princeton University.

Rico-Martínez, R., Anderson, J. S., & Kevrekidis, I. G. (1994b). Continuous-time nonlinear signal processing: a neural network based approach for gray box identification, *Proceedings of the 1994 IEEE Workshop on Neural Networs for Signal Processing* (pp. 596–605). IEEE Publications.

Rico-Martínez, R., Kevrekidis, I. G., & Krischer, K. (1995). Nonlinear system identification using neural networks: dynamics and instabilities. In: Bulsari, A., *Neural networks for chemical engineers* (pp. 409–442). Amsterdam: Elsevier, (Chapter 16).

Robinson, C. (1994). *Dynamical systems: stability, symbolic dynamics, and chaos*. Boca Raton, FL: CRC Press.

Su, H.-T., & McAvoy, T. J. (1991). Identification of chemical processes using recurrent networks. *Proceedings of the 1991 American Control Conference* (pp. 2314–2319).

Takens, F. (1981). Detecting strange attractors in turbulence. In: Rand, D. A., & Young, L. S., *Dynamical systems and turbulence*, Lecture Notes in Mathemathics (pp. 366–381). Heidelberg: Springer.

Tsung, F.-S., & Cottrell, G. W. (1993). Phase-space learning in recurrent networks. *Technical Report CS93-285*, Deptartment of Computer Science & Engineering, University of California, San Diego.

Weigend, A. S., & Gershenfeld, N. A. (1993). *Time series prediction: Forecasting the future and understanding the past*. Reading, MA: Addison-Wesley.

Ydstie, B. E. (1990). Forecasting and control using adaptive connectionist networks. *Computers & Chemical Engineering*, *14*, 583–599.